

1 **Entry of human coronavirus NL63 to the cell.**

2

3 *Running Head: Entry of HCoV-NL63.*

4

5 Aleksandra Milewska<sup>a,b,¶</sup>, Paulina Nowak<sup>a,b,¶</sup>, Katarzyna Owczarek<sup>a,b</sup>, Artur Szczepanski<sup>a,b</sup>,  
6 Mirosław Zarebski<sup>c</sup>, Agnieszka Hoang-Bujnowicz<sup>c</sup>, Krzysztof Berniak<sup>c</sup>, Jacek Wojarski<sup>d</sup>,  
7 Sławomir Zeglen<sup>d</sup>, Zbigniew Baster<sup>e</sup>, Zenon Rajfur<sup>e</sup>, Krzysztof Pyrc<sup>a,b,\*</sup>

8

9 <sup>a</sup> Microbiology Department, Faculty of Biochemistry, Biophysics and Biotechnology,  
10 Jagiellonian University, Gronostajowa 7, 30-387 Krakow, Poland.

11 <sup>b</sup> Laboratory of Virology, Malopolska Centre of Biotechnology, Jagiellonian University,  
12 Gronostajowa 7a, 30-387 Krakow, Poland.

13 <sup>c</sup> Department of Cell Biophysics, Faculty of Biochemistry, Biophysics and Biotechnology,  
14 Jagiellonian University, Gronostajowa 7, 30-387 Krakow, Poland.

15 <sup>d</sup> Department of Cardiac Surgery and Transplantology, Silesian Center for Heart Diseases,  
16 Marii Curie-Skłodowskiej 9, 41-800 Zabrze, Poland.

17 <sup>e</sup> Institute of Physics, Faculty of Physics, Astronomy and Applied Computer Sciences,  
18 Jagiellonian University, Lojasiewicza 11, 30-348 Krakow, Poland.

19

20

21 \* Address correspondence to Krzysztof Pyrc. E-mail: [k.a.pyrc@uj.edu.pl](mailto:k.a.pyrc@uj.edu.pl) www:  
22 <http://virogenetics.info>

23

24 ¶ These authors contributed equally to this work.

25

26 **Abstract**

27 First steps of human coronavirus NL63 (HCoV-NL63) infection were previously  
28 described. The virus binds to target cells by heparan sulfate proteoglycans, and interacts with  
29 the ACE2 protein. Subsequent events, including virus internalization and trafficking, remain  
30 to be elucidated. In this study, we mapped the process of HCoV-NL63 entry into LLC-Mk2  
31 cell line and *ex vivo* 3D tracheobronchial tissue.

32 Using a variety of techniques we have shown that HCoV-NL63 virions require  
33 endocytosis for successful entry to the LLC-MK2 cells, and interaction between the virus and  
34 the ACE2 molecule triggers recruitment of clathrin. Subsequent vesicle scission by dynamin  
35 results in virus internalization, and the newly formed vesicle passes the actin cortex, what  
36 requires active cytoskeleton rearrangement. Finally, acidification of the endosomal  
37 microenvironment is required for successful fusion and release of viral genome into the  
38 cytoplasm. Also for 3D tracheobronchial tissue cultures we observed that the virus enters the  
39 cell by clathrin-mediated endocytosis, but obtained results suggest that this pathway may be  
40 bypassed.

41

42 **Importance**

43 Available data on coronavirus' entry originate frequently from studies employing  
44 immortalized cell lines or undifferentiated cells. Here, using the most advanced 3D tissue  
45 culture system mimicking the epithelium of conductive airways, we systematically mapped  
46 HCoV-NL63 entry into susceptible cell. Obtained data allow for better understanding of the  
47 infection process and may support development of novel treatment strategies.

48

## 49 **Introduction**

50 Human coronavirus NL63 (HCoV-NL63) was discovered shortly after the emergence of  
51 the severe acute respiratory syndrome coronavirus (SARS-CoV) (1). Extensive studies on the  
52 pathogen's biology and epidemiology revealed that it is prevalent worldwide, appearing with  
53 a seasonal distribution similar to that of other human coronaviruses. The clinical presentation  
54 may vary depending on the general health status of the patient. Usually, the virus causes a  
55 relatively mild respiratory tract disease, but fatal cases have been reported (2-5). Furthermore,  
56 broad studies on the association between infection and clinical symptoms reveal that  
57 HCoV-NL63 is associated with croup in young children (6-9).

58 Phylogenetically, HCoV-NL63 clusters within the genus alphacoronavirus, which also  
59 includes another human pathogen, HCoV-229E. Initially, these two viruses were considered  
60 distant relatives that diverged at some point due to an unknown reason. More recent research  
61 shows, however, that these two species most likely emerged in the human population during  
62 two separate zoonotic transmission events (10-12).

63 From the perspective of genome structure, HCoV-NL63 is similar to other  
64 alphacoronaviruses in that the 5' terminal two-thirds of the genome encode a large  
65 polyprotein, which is cleaved to yield several non-structural proteins. Five genes (S-ORF3-E-  
66 M-N) are located at the 3' terminus encode structural proteins. The spike protein (S) is a class  
67 I fusion protein comprising a rod-like domain anchored to the virion via its C-terminus, and a  
68 globular head responsible for the interaction with cellular entry receptors (13). It is generally  
69 assumed that alphacoronaviruses interact with and enter host cells using the CD13  
70 (aminopeptidase N). However, HCoV-NL63 utilizes the ACE2 protein for this purpose, a  
71 characteristic shared only with SARS-CoV (14, 15). Virus tropism not only depends on the  
72 presence of a certain entry receptor but also may be modulated by other factors, e.g.,

73 attachment receptors, protease availability, and the activity of pathways responsible for  
74 internalization and trafficking of the virus particle (16, 17).

75 While binding to their cognate entry receptor provides sufficient stimulus for some  
76 viruses to initiate fusion between the viral and cellular membranes, most internalize *via*  
77 endocytosis; acidification and/or processing by cathepsins is then a pre-requisite for fusion  
78 (13). For a long time, endocytic entry of virions was classified as clathrin-dependent, clathrin-  
79 independent, or clathrin- and caveolin-independent. During recent years, a number of other  
80 pathways were identified and this complex machinery has become better understood. The  
81 occurrence, abundance, and mechanistic details of these pathways appear to vary between cell  
82 types, tissues, and species. Most often, the selection of a specific endocytic route is linked to  
83 cargo-directed trafficking and receptor-dependent trafficking. Nevertheless, many  
84 receptors/cargoes allow flexibility due to their capacity to enter a cell *via* multiple pathways.

85 The early stages of HCoV-NL63 infection have been described by us and others (18-  
86 20). Here, we made an effort to delineate events that occur early during HCoV-NL63  
87 infection. First, the virus anchors to ciliated cells *via* heparan sulfate proteoglycans before  
88 interacting with the ACE2 entry receptor. Our results show that the virus-ACE2 interaction  
89 triggers recruitment of clathrin, followed by clathrin-mediated, dynamin-dependent  
90 endocytosis, which requires actin cortex remodeling. To ensure that our results were reliable,  
91 we used *ex vivo* cultured human airway epithelium (HAE), which mimics the  
92 microenvironment at the infection site.

93 **Results**

94 **HCoV-NL63 enters the cell via endocytosis**

95 We first determined whether entry of HCoV-NL63 requires endocytosis and  
96 acidification of endosomes. For this, we studied the effect of ammonium chloride (NH<sub>4</sub>Cl)  
97 and bafilomycin A - lysosomotropic agents that inhibit acidification of endosomes (21-23)  
98 using two models of HCoV-NL63 infection: permissive LLC-Mk2 cells and HAE cultures.  
99 Cells were pre-incubated with NH<sub>4</sub>Cl (50 mM), bafilomycin A (100 nM) or control DMSO  
100 for 1 h at 37°C, and subsequently incubated with the virus at TCID<sub>50</sub> of 100/ml (for LLC-Mk2  
101 cells) or at TCID<sub>50</sub> of 400/ml (for HAE) for 2 h at 32°C in the presence of the inhibitor.  
102 Subsequently, supernatants were removed and cells were washed thrice with acidic buffer to  
103 inhibit the fusogenic activity of the virions retained on the surface (24). Next, LLC-Mk2 cells  
104 were washed with 1 × PBS (pH 7.4), overlaid with culture medium and incubated at 32°C for  
105 4 days. Supernatant samples were collected for virus replication analysis. Simultaneously,  
106 HAE cultures were washed with 1 × PBS (pH 7.4) and further maintained at an air-liquid  
107 interphase at 32°C for 5 days. During this time HAE cultures were washed every 24 h with  
108 1 × PBS supplemented with a given inhibitor for 10 min at 32°C, and apical washes were  
109 collected for virus replication analysis. Subsequently, viral RNA was isolated, reverse  
110 transcribed (RT), and HCoV-NL63 yield was determined using a quantitative real-time PCR  
111 (qPCR).

112 Bafilomycin A and NH<sub>4</sub>Cl inhibited HCoV-NL63 infection in LLC-Mk2 cells, proving  
113 that acidification is a pre-requirement for the virus infection *in vitro*. No inhibition was  
114 observed in HAE cultures (**Fig. 1A**). No cytotoxic effect was observed in the presence of  
115 these inhibitors (**Fig. 1B**).

116 Next, we analyzed HCoV-NL63 co-localization with the early endosome antigen-1  
117 (EEA1), a hydrophilic protein localizing exclusively to early endosomes (25). LLC-Mk2 cells

118 were fixed after 10, 20, 30 or 40 min post-inoculation (p.i.) with gradient-purified virus,  
119 stained with antibodies specific to HCoV-NL63 N protein and EEA1, and analyzed under  
120 confocal microscope. Measured co-localization expressed as Manders' coefficient increases  
121 with time and reaches 0.68 forty min p.i. (n = 6 cells) (**Fig. 1C**).

122 We validated the obtained results using the HAE model. Briefly, HAE cultures were  
123 inoculated with gradient-purified HCoV-NL63 and incubated at 32°C for 2 h. For this culture  
124 model a longer incubation was required to observe virus attachment and entry, most likely due  
125 to the requirement to cross the mucus layer. Subsequently, cells were fixed and labeled with  
126 specific antibodies against HCoV-NL63 N protein and EEA1. Co-localization of HCoV-NL63  
127 virus particles with EEA1 protein was analyzed using confocal microscope. Co-localization of  
128 virus and EEA1 was observed in inoculated cells (**Fig. 1D**).

129

### 130 **Endocytosis of virus particles is induced by binding to the entry receptor**

131 HCoV-NL63 virus employs the ACE2 protein for cellular entry, while heparan sulfate  
132 proteoglycans serve as attachment receptors (19). Here, we analyzed the consequence of  
133 interaction between the virus particle and ACE2. First, we inoculated naturally permissive  
134 LLC-Mk2 cells with HCoV-NL63 and incubated for 40 min at 4°C to enable virus adhesion  
135 to a cell surface. Subsequently cells were fixed, the virus was labelled with specific antibodies  
136 and its co-localization with the ACE2 and clathrin was studied. As shown in **Fig. 2A**,  
137 HCoV-NL63 particles attach efficiently to the cell surface. However, only a proportion of  
138 virions co-localize with the ACE2 (Manders'coeff. = 0.573; n = 5), suggesting that binding to  
139 the HS precedes interaction with the entry receptor. At that point, there is no co-localization  
140 of virus particles and clathrin-coated pits (Manders'coeff. = 0.140; n = 5) (**Fig. 2B**). Next, we  
141 tested whether the virus binding to the adhesion or entry receptor triggers recruitment of  
142 common cellular proteins responsible for pit formation by incubating cells for 5 min at 32°C.

143 Immunostaining showed that the virus particles bound to the ACE2 start to co-localize with  
144 clathrin (Manders'coeff. = 0.849, n = 6) (**Fig. 2C**), while there is no co-localization between  
145 non-ACE2-bound virions and clathrin (Manders'coeff. = 0.189, n = 6).

146

#### 147 **HCoV-NL63 co-localizes with clathrin during entry**

148 To determine whether co-localization with clathrin following the ACE2 binding is  
149 relevant, and indeed the virus enters the cell by clathrin-coated pits we analyzed  
150 co-localization of intracellular virions with clathrin. Briefly, LLC-Mk2 cells were incubated at  
151 32°C for 5-20 min with gradient-purified HCoV-NL63, fixed, immunostained and analyzed  
152 with confocal microscopy. Results showed co-localization of virions entering the cell with  
153 clathrin (Manders'coeff. = 0.584; n = 7) (**Fig. 3A**), whereas no co-localization with caveolin-1  
154 was observed (Manders'coeff. = 0.053; n = 5) (**Fig. 3B**). HCoV-NL63 co-localization with  
155 clathrin and caveolin was also studied in HAE model. For this, cultures were incubated with  
156 gradient-purified HCoV-NL63 at 32°C for 2 h; the virus and the cellular proteins were  
157 immunostained and analyzed with confocal microscopy. HCoV-NL63 virions also in this  
158 model co-localized with clathrin, whereas no co-localization was observed for caveolin-1  
159 (**Fig. 3**).

160

#### 161 **Clathrin and dynamin are important for HCoV-NL63 entry**

162 As we already knew that HCoV-NL63 virions migrate to clathrin-coated pits, in the  
163 subsequent step we aimed to determine whether the clathrin-mediated endocytosis is indeed  
164 important for the virus entry. For this reason, we blocked the pathway using Pitstop 2 (N-[5-  
165 [4-Bromobenzylidene]-4-oxo-4,5-dihydro-1,3-thiazol-2-yl] naphthalene-1-sulfonamide) – a  
166 selective clathrin inhibitor targeting its amino terminal domain, and MitMAB  
167 (tetradecyltrimethylammonium bromide) – a dynamin I and II GTPase inhibitor. Activity of

168 these compounds was verified with the positive control (fluorescently-labelled transferrin)  
169 (26, 27). LLC-Mk2 cells were treated with Pitstop 2, MitMAB or control DMSO for 30 min  
170 at 37°C, following transferrin uptake for 45 min at 37°C. Confocal images showed that both  
171 inhibitors blocked transferrin endocytosis, as the protein was present only on the cell surface  
172 (**Fig. 4A-D**).

173 Subsequently, LLC-Mk2 cells were incubated with one of the inhibitors at 37°C for  
174 30 min and inoculated with gradient-purified HCoV-NL63 at 32°C for 5 min. Following  
175 immunostaining of the HCoV-NL63 N protein and actin, virus endocytosis was analyzed  
176 using confocal microscopy. Results showed that virus internalization was hampered in cells  
177 pre-treated with clathrin and dynamin inhibitors, as compared to the DMSO-treated cells  
178 (**Fig. 4D-G**). Simultaneously, a cytotoxicity test of the entry inhibitors was performed, which  
179 showed no toxic effect of the tested compounds to LLC-Mk2 cells (**Fig. 5**). In order to ensure  
180 that our observations are not biased, statistical analysis of virus entry was performed. For this,  
181 an algorithm was prepared for image analysis and 3D representation of the cell was prepared  
182 and virus position in the cell was determined (**Fig. 6**).

183 Similar experiment was conducted using HAE cultures. For this, cultures were  
184 incubated for 1 h at 37°C with inhibitors described above, following incubation with gradient-  
185 purified HCoV-NL63 at 32° C for 2 h. A strong inhibition of virus internalization in cultures  
186 pre-incubated with clathrin or dynamin inhibitors was observed, compared to control cells  
187 (**Fig. 7**). No cytotoxicity to HAE was observed for the tested inhibitors after 3 h incubation at  
188 37°C (**Fig. 8**).

189

#### 190 **Clathrin mediated endocytosis is the main entry route for HCoV-NL63**

191 Even though certain cargo is usually internalized by a single route, frequently other  
192 pathways may be used as alternatives. We therefore aimed to test whether inhibition of

193 clathrin-mediated entry with chemical inhibitors results in inhibition of virus replication. To  
194 address this, we incubated LLC-Mk2 cells with a given inhibitor at 37° C for 1 h and infected  
195 them with HCoV-NL63 (TCID<sub>50</sub> = 400 per ml) for 2 h at 32°C. Subsequently media were  
196 removed and cells were washed thrice with acidic buffer, following washing with 1 × PBS  
197 (pH 7.4). Next, cells were overlaid with culture medium containing a given inhibitor and  
198 incubated at 32°C for 4 days. Cells were fixed and immunostained for HCoV-NL63 N protein  
199 to assess the number of infected cells. To assess the non-specific effect of entry inhibitors,  
200 control cells were treated with these also 4 h p.i. Clearly, in the presence of clathrin-mediated  
201 endocytosis inhibitors (Pitstop 2 and MitMAB) the number of HCoV-NL63-infected cells was  
202 much lower compared to the control. However, MitMAB also inhibited virus replication at  
203 later stages of the infection (**Fig. 9**). To ensure that entry inhibitors affected HCoV-NL63  
204 infection in LLC-Mk2 cells, we analyzed by RT-qPCR virus replication at 120 h p.i. in the  
205 presence of tested compounds. The analysis showed a ~2-log decrease in virus progeny  
206 production in the presence of Pitstop 2 and MitMAB, compared to DMSO-treated cells and a  
207 slight increase of RNA copy levels in the presence of nystatin (**Fig 10A**). Importantly, no  
208 cytotoxic effect was observed for the tested inhibitors applied to LLC-Mk2 for 4 days at 32°C  
209 (**Fig 10B**). The influence of tested inhibitors on HCoV-NL63 infection was analyzed also in  
210 HAE cultures. For this, cultures were pre-incubated with a given inhibitor (Pitstop 2,  
211 MitMAB, nystatin or control DMSO) for 1 h at 37°C and infected with HCoV-NL63 at  
212 TCID<sub>50</sub> of 400 per ml for 2 h at 32°C. Subsequently, non-internalized virions were inactivated  
213 by acid wash, cultures were washed with 1 × PBS, and incubated with a given inhibitor for 10  
214 min. After that time supernatants were discarded and cultures were incubated for 5 days at  
215 32°C. During this period, cultures were incubated with a given inhibitor for 10 min at 32°C  
216 every 24 h. Viral RNA from these samples was quantified by RT-qPCR. Virus replication in  
217 HAE was not affected by any of the tested inhibitors (**Fig. 10A**).

218

**219 TMPRSS2 is important during early stages of the infection**

220 It was previously suggested that coronaviruses may bypass the endocytic entry route  
221 employing TMPRSS2 protease, which primes the fusion protein and enable fusion of viral  
222 and cellular membranes on the cell surface (31, 32). We have tested whether inhibition of the  
223 TMPRSS2 proteases with camostat affects the HCoV-NL63 infection. We observed that  
224 inhibition of TMPRSS2 protease hampers virus infection in HAE cultures, while it has no  
225 effect on virus replication in LLC-MK2 cells (**Fig. 11A**). No inhibition of virus entry was  
226 observed in any of the models, as tracked with confocal microscopy, visualizing the  
227 nucleoprotein (**Fig. 11B**). As only single entry events per view were observed, several images  
228 for camostat-treated and control cells are presented. In total, 500 entry events into HAE cells  
229 were tracked and no difference between the camostat-treated sample and control sample was  
230 noted.

231

**232 HCoV-NL63 entry requires actin re-modelling**

233 We studied trafficking of HCoV-NL63 inside the cell. As entry by endocytosis would  
234 probably require re-modelling of the cytoskeleton, we evaluated virus internalization in the  
235 presence of cytochalasin D, jasplankinolide or nocodazole. The first chemical inhibits actin  
236 polymerization, whereas the second binds F-actin and stabilizes actin filaments (33, 34). The  
237 last compound interferes with the microtubule formation. The analysis showed that actin  
238 inhibitors prevented virus particles from penetrating the cell, with visible viral particles  
239 accumulation on actin cortex or unstructured actin deposits. Microtubule inhibitor did not  
240 affect virus entry (**Fig. 12**). No cytotoxicity was observed for the tested inhibitors (**Fig. 13**).

241 **Discussion**

242 Previously, we and others described the first steps of the HCoV-NL63 infection process,  
243 showing that it begins with the virus binding to the cellular membrane *via* heparan sulfate  
244 proteoglycans, which then enable/facilitate interaction with the entry receptor, ACE2 (14, 18,  
245 19). Little is known about the subsequent virus internalization and its trafficking through the  
246 cytoplasm, and some published data are contradictory. For example, the role played by  
247 cathepsins and acidification of the microenvironment during transition of the HCoV-NL63 S  
248 protein to its fusogenic form remains unclear.

249 We made an effort to systematically examine every step of the process. First, we tested  
250 whether the virus requires endocytosis for successful entry. To do this, we carried out  
251 experiments using chemical inhibitors of endosome acidification (ammonium chloride and  
252 bafilomycin A). Both blocked virus infection in LLC-MK2 cells, suggesting a requirement for  
253 transport of virions to endosomes, which then undergo acidification. Yet, such an approach  
254 may have several disadvantages. First, we examined the role of endosome acidification based  
255 on virus replication; thus we cannot rule out interference with virus infection at later stages  
256 (as shown for MiTMAB). Second, the specificity and selectivity of chemical inhibitors are  
257 questionable. An indirect proof for the pH dependence of HCoV-NL63 entry may be provided  
258 by the fact that acidification of the environment (acid wash) results in inactivation of the  
259 virus, suggesting the pH – directed structural switch in the S protein. To further confirm our  
260 observations, we developed a method of visualizing single virions as they entered the cell.  
261 Efforts to stain for virus surface proteins yielded poor results, most likely due to lack of  
262 highly specific antibodies and post-translational modification of surface proteins and the best  
263 results were obtained when antibodies specific to the N protein were used. Incubation of cells  
264 with purified virions resulted in virus attachment, which was visualized by confocal  
265 microscopy and co-staining for markers of the most commonly employed endocytic pathways

266 allowed us to study the co-localization. If significant co-localization was detected, results  
267 were confirmed with chemical inhibitors.

268 The results showed that HCoV-NL63 binding to the ACE2 initiates recruitment of  
269 clathrin and subsequent formation of clathrin coated pits; no co-localization of the virus with  
270 other markers (e.g., caveolin) was noted. Transferrin was used as a positive control for  
271 clathrin-mediated endocytosis (35, 36). Importantly, chemical inhibitors of clathrin  
272 completely blocked virus internalization and the virus remained on the cell surface. Analysis  
273 of HAE cultures yielded identical results. The inhibitors of endocytosis also hampered virus  
274 infection on LLC-Mk2 cells, highlighting that this pathway is relevant and the lack of an  
275 equally effective alternative entry route in this culture model. Clathrin-mediated endocytosis  
276 requires a number of other proteins, as dynamin, the GTPase responsible for scission of  
277 clathrin-coated vesicles from the cell surface (37). Inhibiting dynamin also hampered virus  
278 internalization into LLC-MK2 cells and HAE cultures, confirming our previous observations.  
279 However, in this case the MitMAB compound blocked replication of HCoV-NL63 also during  
280 subsequent stages of the infection.

281 It is noteworthy that we were not able to block virus infection of HAE cultures using  
282 inhibitors of endocytosis. This may be related to the fact that the cultures were exposed to  
283 inhibitors for a very short time during apical washes, which is not sufficient to permanently  
284 block the infection. On the other side, it is also possible that in HAE HCoV-NL63 is able to  
285 enter the cell by an alternative route. Recent reports on other coronaviruses (31, 32, 38)  
286 suggested that these viruses may bypass the endocytic entry route using TMPRRS2 as the  
287 priming protease, enabling the entry directly from the cell surface. Our experiments showed  
288 that inhibition of this protease indeed inhibited virus infection. Interestingly, it did not hamper  
289 virus internalization to the cell. Our data are consistent with the data presented by others (31,  
290 32, 38), yet we believe that there is a different mechanistic explanation to the observed

291 phenomenon. We believe that indeed TMPRRS2 protease is required for the virus-cell fusion,  
292 acting similarly to cathepsins, but it does not enable fusion on the cell surface and the  
293 acidification of the microenvironment is required.

294 Our final research question was about virus trafficking. The endosome typically  
295 translocates through the depolymerizing actin cortex and is subsequently sorted at the  
296 endosomal hub and directed to different destinations. This sorting is highly dependent on the  
297 cargo. Using two chemical inhibitors (jasplankinolide and cytochalasin B) (34, 39), we  
298 showed that actin plays a vital role in virus entry. Stabilization of the actin cortex using  
299 jasplankinolide similarly as inhibition of actin polymerization using cytochalasin D resulted in  
300 immobilization of the virus at the cell surface. These two experiments suggest a scenario in  
301 which virus-carrying endosomes pass along the actin cortex, which actively unwinds and  
302 interacts with virions.

303 Summarizing, we show that HCoV-NL63 enters the cell by clathrin-mediated  
304 endocytosis, but the pathway may be bypassed to some extent during the infection *ex vivo*.  
305 HCoV-NL63 entry to the susceptible cell was summarized in **Fig 14**.

306 **Materials and methods**

307 **Cell culture**

308 LLC-Mk2 cells (ATCC: CCL-7; *Macaca mulatta* kidney epithelial) were maintained in  
309 minimal essential medium (MEM; two parts Hanks' MEM and one part Earle's MEM;  
310 Thermo Scientific, Poland) supplemented with 3% heat-inactivated fetal bovine serum  
311 (Thermo Scientific, Poland), penicillin (100 U/ml), streptomycin (100 µg/ml), and  
312 ciprofloxacin (5 µg/ml). Cells were cultured at 37°C under 5% CO<sub>2</sub>.

313

314 **Ethics Statement**

315 Human tracheobronchial epithelial cells were obtained from airway specimens resected  
316 from adult patients undergoing surgery under Silesian Center for Heart Diseases-approved  
317 protocols. This study was approved by the Bioethical Committee of the Medical University of  
318 Silesia in Katowice, Poland (approval no: KNW/0022/KB1/17/10 dated on 16.02.2010).  
319 Participants provided their written informed consent to participate in the study, as approved  
320 by the Bioethical Committee.

321

322 **Human airway epithelium cultures**

323 Primary human tracheobronchial epithelial cells were expanded on plastic to generate  
324 passage 1 cells and plated on permeable Transwell inserts (6.5 mm-diameter) supports.  
325 Human airway epithelium (HAE) cultures were generated by provision of an air-liquid  
326 interface for 6-8 weeks to form well-differentiated, polarized cultures that  
327 resemble *in vivo* pseudostratified mucociliary epithelium. Cultures were prepared and  
328 maintained as previously described (24).

329

### 330 **Cell viability assay**

331 LLC-Mk2 cells were cultured on 96-well plates and HAE cultures were prepared as  
332 described above. Cell viability assay was performed by using the XTT Cell Viability Assay  
333 (Biological Industries, Israel), according to the manufacturer's instructions. Briefly, on the  
334 day of the assay 100  $\mu$ l of the culture medium (for LLC-Mk2) or 1  $\times$  PBS (for HAE) with the  
335 30  $\mu$ l of the activated XTT solution was added to each well/culture insert. Following 2 h  
336 incubation at 37°C, the solution was transferred onto a 96-well plate and signal was measured  
337 at  $\lambda = 490$  nm using the colorimeter (Spectra MAX 250, Molecular Devices). The obtained  
338 results were further normalized to the control sample, where cell viability was set to 100%.

339

### 340 **Virus preparation and titration**

341 The HCoV-NL63 stock (isolate Amsterdam 1) was generated by infecting monolayers  
342 of LLC-Mk2 cells. The virus-containing liquid was aliquoted and stored at  $-80^{\circ}\text{C}$ . A control  
343 LLC-Mk2 cell lysate from mock-infected cells was prepared in the same manner. The virus  
344 yield was assessed by titration on fully confluent LLC-Mk2 cells in 96-well plates, according  
345 to the method described by Reed and Muench (40).

346

### 347 **Purification of HCoV-NL63**

348 The virus stock was concentrated 25-fold using centrifugal protein concentrators  
349 (Amicon Ultra, 10 kDa cut-off; Merck, Poland) and subsequently overlaid on 15% iodixanol  
350 solution in 1  $\times$  PBS (OptiPrep medium; Sigma-Aldrich, Poland). Following virus  
351 concentration using iodixanol cushion (centrifugation at  $175\,000 \times g$  for 3 h at  $4^{\circ}\text{C}$ ) it was  
352 overlaid on 10-20% iodixanol gradient in 1  $\times$  PBS and centrifuged at  $175\,000 \times g$  for 18 h at  
353  $4^{\circ}\text{C}$ . Fractions (1 ml) collected from the gradient were analyzed on western blot, using  
354 anti-HCoV-NL63 N IgGs (0.25  $\mu\text{g/ml}$ ; Ingenansa, Spain) and a secondary antibody coupled

355 with horseradish peroxidase (65 ng/ml, Dako, Denmark). The virus-containing fractions were  
356 aliquoted and stored at  $-80^{\circ}\text{C}$ . The control cell lysate (mock) was concentrated and prepared  
357 in the same manner as the virus stock.

358

### 359 **Inhibition of virus entry**

360 LLC-Mk2 cells were seeded on coverslips in six-wells plates (TPP) and cultured for  
361 2 days at  $37^{\circ}\text{C}$ . Subsequently, cells were incubated with a given inhibitor for 30 min at  $37^{\circ}\text{C}$ ,  
362 and later with 50  $\mu\text{l}$  of purified HCoV-NL63 or mock sample for 1 h at  $32^{\circ}\text{C}$ . For the *ex vivo*  
363 experiment, HAE cultures were exposed to the tested inhibitor or control PBS for 1 h at  $37^{\circ}\text{C}$ ,  
364 following inoculation with iodixanol-concentrated HCoV-NL63 or mock sample. Following  
365 2 h incubation at  $32^{\circ}\text{C}$ , unbound virions were removed by washing with  $1 \times \text{PBS}$ . Cells were  
366 then washed with  $1 \times \text{PBS}$  and fixed with 4% paraformaldehyde (PFA).

367 Transferrin and albumin were used as positive controls, as they were previously  
368 described to serve as a cargo in the clathrin- and caveolin- dependent endocytosis,  
369 respectively (41, 42). LLC-Mk2 cells were seeded on coverslips in six-wells plates (TPP,  
370 Switzerland) and cultured for 2 days at  $37^{\circ}\text{C}$ . Subsequently, cells were incubated with a given  
371 inhibitor for 30 min at  $37^{\circ}\text{C}$ , following incubation with Alexa Fluor 488-labeled transferrin  
372 (100  $\mu\text{g}/\text{ml}$ ; Molecular Probes) or FITC labeled albumin (500  $\mu\text{g}/\text{ml}$ ; Sigma-Aldrich, Poland)  
373 or control PBS for 45 min at  $32^{\circ}\text{C}$ . Cells were then washed with  $1 \times \text{PBS}$  and fixed in  
374 4% PFA.

375

### 376 **Immunostaining and confocal imaging**

377 Fixed cells were permeabilized with 0.1% Triton X-100 in  $1 \times \text{PBS}$  and incubated  
378 overnight at  $4^{\circ}\text{C}$  in  $1 \times \text{PBS}$  supplemented with 5% BSA and 0.5% Tween 20. To visualize  
379 HCoV-NL63 particles, cells were incubated for 2 h at room temperature with mouse

380 anti-HCoV-NL63 N IgGs (0.25 µg/ml; Ingenansa, Spain), followed by a 1 h incubation with  
381 Alexa Fluor 488-labeled goat anti-mouse IgG (2.5 µg/ml; Thermo Scientific, Poland). The  
382 following antibodies were used for endosomal markers: polyclonal goat anti-human  
383 clathrin HC coupled with tetramethylrodamine (10 µg/ml; Santa Cruz Biotechnology) and  
384 polyclonal rabbit anti-human early endosome antigen 1 (2 µg/ml; Santa Cruz Biotechnology);  
385 polyclonal rabbit anti-human caveolin-1 (2 µg/ml; Sigma-Aldrich, Poland), and Alexa Fluor  
386 633-labeled goat anti-rabbit (2.5 µg/ml; Thermo Scientific, Poland). Actin filaments was  
387 stained using phalloidin coupled with Alexa Fluor 633 (0.2 U/ml; Thermo Scientific, Poland).  
388 Nuclear DNA was stained with DAPI (0.1 µg/ml; Sigma-Aldrich, Poland). Immunostained  
389 cultures were mounted on glass slides in ProLong Gold antifade medium (Thermo Scientific,  
390 Poland). Fluorescent images were acquired under a Leica TCS SP5 II confocal microscope  
391 (Leica Microsystems GmbH, Mannheim, Germany) and a Zeiss LSM 710 confocal  
392 microscope (Carl Zeiss Microscopy GmbH). Images were acquired using Leica Application  
393 Suite Advanced Fluorescence LAS AF v. 2.2.1 (Leica Microsystems CMS GmbH) or ZEN  
394 2012 SP1 software (Carl Zeiss Microscopy GmbH), respectively, deconvolved with Huygens  
395 Essential package ver. 4.4 (Scientific Volume Imaging B.V.; The Netherlands) and processed  
396 using ImageJ 1.47v (National Institutes of Health, Bethesda, Maryland, USA).

397

### 398 **Flow cytometry**

399 LLC-Mk2 cells were seeded on 6-wells plates (TPP), cultured for 2 days at 37°C with  
400 5% CO<sub>2</sub>. Cells in monolayer were incubated with each entry inhibitor for 1 h at 37°C,  
401 following infection with HCoV-NL63 at TCID<sub>50</sub> of 100/ml or inoculation of the mock  
402 sample. On day 4 p.i., cells were washed with sterile PBS, fixed with 3% PFA, permeabilized  
403 with 0.1% Triton X-100 in 1 × PBS and incubated for 1 h with 3% BSA in 1 × PBS with  
404 0.1% Tween 20. To quantify HCoV-NL63 infection, fixed cells were scraped from plastic and

405 incubated for 2 h at room temperature with mouse anti-HCoV-NL63 N IgG antibodies (1  
406  $\mu\text{g/ml}$ ; Ingenansa), followed by 1 h incubation with Alexa Fluor 488-labeled goat anti-mouse  
407 antibody (2.5  $\mu\text{g/ml}$ ; Molecular Probes). Cells were then washed, re-suspended in  $1 \times \text{PBS}$   
408 and analyzed with FACS Calibur (Becton Dickinson) using Cell Quest software.

409

#### 410 **Isolation of nucleic acids and reverse transcription**

411 Viral nucleic acids were isolated from cell culture supernatants (LLC-Mk2 cells) or  
412 apical washes (HAE cultures) using the Viral RNA/DNA Isolation Kit (A&A Biotechnology,  
413 Poland), according to the manufacturer's instructions. Reverse transcription was carried out  
414 with a High Capacity cDNA Reverse Transcription Kit (Thermo Fisher Scientific, Poland),  
415 according to the manufacturer's instructions.

416

#### 417 **Quantitative RT-PCR**

418 HCoV-NL63 yield was determined using an RT-qPCR (7500 Fast Real-Time PCR  
419 machine, Life Technologies, Poland). Viral cDNA (2.5  $\mu\text{l}$  per sample) was amplified in a  
420 10  $\mu\text{l}$  reaction mixture containing  $1 \times \text{Master Mix}$  (RT Mix Probe, A&A Biotechnology,  
421 Poland), specific probe labelled with 6-carboxyfluorescein (FAM) and 6-  
422 carboxytetramethylrhodamine (TAMRA) (100 nM; 5'-ATG TTA TTC AGT GCT TTG GTC  
423 CTC GTG AT- 3') and primers (450 nM each; sense: 5'-CTG TGG AAA ACC TTT GGC  
424 ATC- 3'; antisense: 5' – CTG TGG AAA ACC TTT GGC ATC- 3'). Rox was used as the  
425 reference dye. The reaction conditions were as follows: 2 min at 50°C and 10 min at 92°C,  
426 followed by 40 cycles of 15 sec at 92°C and 1 min at 60°C. In order to assess the copy  
427 number for the N gene, DNA standards were prepared. Briefly, N gene of HCoV-NL63 was  
428 amplified and cloned into pTZ57R/T (Thermo Fisher Scientific, Poland) plasmid using the  
429 InsTAclone PCR cloning kit (Thermo Scientific, Poland). Subsequently, DNA vectors were

430 amplified and linearized with *EcoRI* restriction enzyme. Linear nucleic acids were further  
431 purified with the GeneJET™ PCR Purification Kit (Thermo Fisher Scientific, Poland),  
432 according to the manufacturer's instructions and its concentration was assessed using a  
433 spectrophotometer. The number of DNA copies/ml was assessed using Avogadro's constant  
434 and molecular mass of RNA molecules. Samples were serially diluted and used as an input  
435 real-time PCR reaction.

436 In this article, the data from quantitative PCR are presented as log removal values  
437 (LRVs) in order to enable comparison of results obtained from different assays. LRV was  
438 calculated according to the following formula:  $LRV = -\log (c_i/c_0)$  where  $c_i$  is the number of  
439 viral RNA copies per milliliter in the sample in the culture treated with a given polymer and  
440  $c_0$  is the number of viral RNA copies per milliliter in control sample (untreated cells).

441

#### 442 **Image analysis**

443 To evaluate the infection inhibition in the presence of various endocytosis inhibitors  
444 image analysis was performed on 2 mm × 2 mm tile scan images. On each image, the number  
445 of nuclei (expressed as a number of cells) and the mean pixel intensity for the virus were  
446 calculated. For that, histograms of all images were adjusted to the min/max value, excluding  
447 signal from the virus derived from images with no infected cells. Results are presented as  
448 mean intensity of fluorescence per cell.

449 Co-localization analyses were performed under ImageJ using JACoP plugin (Bolte and  
450 Cordelieres, 2006), where Manders' coefficient was calculated for 3D images of more than  
451 5 cells.

452 Quantitative analysis of virus internalization in the presence of inhibitors was performed  
453 with algorithm previously described by Berniak *et al.* with modifications (43). Cell surface  
454 was estimated on each image slice manually using polygon selection tool in ImageJ and based

455 on this information 3D cell surface was modelled. Coordinates of virus particles were  
456 determined using 3D Object Counter ImageJ plugin. Relative localization and distance  
457 between virus particle and cell surface was calculated. Results are presented as a ratio  
458 between virus particles inside a cell and the particles on the surface (up to 1.5  $\mu\text{m}$  above).

459

#### 460 **Statistical analysis**

461 All the experiments were performed in triplicate and the results are presented as mean  
462  $\pm$  SD. To determine significance of the obtained results, a comparison between groups was  
463 conducted using the Student's t-test. *P* values  $< 0.05$  were considered significant.

464

465 **ACKNOWLEDGMENTS**

466 This work was supported by grants from the National Science Center (UMO-  
467 2012/07/E/NZ6/01712 and UMO-2012/07/N/NZ6/02955 and 2015/19/N/NZ1/00323) (KP  
468 and AM and KB, respectively) and the Ministry of Science and Higher Education  
469 0058/DIA/2015/44 (PN).

470 KP would like to acknowledge networking contribution by the COST Action CM1407  
471 “Challenging organic syntheses inspired by nature - from natural products chemistry to drug  
472 discovery”.

473 The Faculty of Biochemistry, Biophysics and Biotechnology of the Jagiellonian University is  
474 a beneficiary of the structural funds from the European Union (grant No: POIG.02.01.00-12-  
475 064/08 – “Molecular biotechnology for health”).

476 Faculty of Biochemistry, Biophysics and Biotechnology of the Jagiellonian University is a  
477 partner of the Leading National Research Center supported by the Ministry of Science and  
478 Higher Education of the Republic of Poland.

479 The funders had no role in study design, data collection and analysis, decision to publish, or  
480 preparation of the manuscript.

481



483 **Figure legends**

484 **Fig 1. Importance of endosomal entry for HCoV-NL63 infection.**

485 (A) Inhibition of HCoV-NL63 infection in LLC-Mk2 cells and HAE cultures by  
486 lysosomotropic agents: ammonium chloride (NH<sub>4</sub>Cl, 50 mM) and bafilomycin A (Baf A,  
487 100 nM), as determined with a RT-qPCR; values on the y axis are presented as LRV. The  
488 assay was performed in triplicate, and average values with standard errors are presented. *P*  
489 values < 0.05 were considered significant and are denoted with an asterisk (\*). (B)  
490 Cytotoxicity of the tested inhibitors was measured with an XTT assay. Data on the y-axis  
491 represent viability of the treated cells compared to the untreated reference samples. The assay  
492 was performed in triplicate and average values with standard errors are presented. (C, D)  
493 Confocal images showing co-localization of HCoV-NL63 virions with early endosomal  
494 marker EEA1 on LLC-Mk2 cells (C) and HAE cultures (D). Scale bar = 5 μm. Green:  
495 HCoV-NL63, red: EEA1.

496

497 **Fig 2. HCoV-NL63 binding to the ACE2 triggers clathrin-mediated endocytosis.**

498 Pre-cooled LLC-Mk2 cells were incubated with gradient-purified HCoV-NL63 for 40 min at  
499 4°C, following 0 min (A, B) or 5 min (C) incubation at 32°C. Co-localization of the virus  
500 (green) and the ACE2 (red) was analyzed using confocal microscopy (A). No colocalisation  
501 with clathrin was observed after 0 min incubation (B). Triple co-localization of virus with  
502 ACE2 and clathrin (blue) is visible in panel (C). Images on the right side are zoomed-in  
503 regions indicated by white rectangles on the left-side slides. A representative image is shown.  
504 Scale bar = 10 μm.

505

506 **Fig 3. HCoV-NL63 co-localizes with clathrin, but not caveolin.**

507 LLC-Mk2 cells were incubated with gradient-purified HCoV-NL63 for 40 min at 4°C,  
508 following 5 min (A) or 20 min (B) incubation at 32°C. HAE cultures were incubated with  
509 gradient-purified HCoV-NL63 for 40 min at 4°C, following 120 min incubation at 32°C.  
510 HCoV-NL63 co-localization with clathrin (A) or caveolin (B) was analyzed with confocal  
511 microscopy (HCoV-NL63: green, clathrin and caveolin: red, nuclei: blue). Cells incubated  
512 with mock and stained with isotypic antibodies were used as control (C). Scale bar = 5 µm.

513

514 **Fig 4. Clathrin and dynamin inhibitors hamper internalization of HCoV-NL63.**

515 In order to verify effectiveness of inhibitors, LLC-Mk2 cells were incubated with control  
516 DMSO (A), 10 µM Pitstop 2 (B), or 10 µM MitMAB (C) for 30 min at 37°C, and inoculated  
517 with Alexa Fluor-488-labelled transferrin. Following incubation (45 min, 37°C), cells were  
518 fixed and stained for actin (red). Transferrin entry was evaluated with confocal microscopy.  
519 Further, LLC-Mk2 cells were incubated with control DMSO (E), 10 µM Pitstop 2 (F), 10 µM  
520 MitMAB (G) for 30 min at 37°C. Cells were inoculated with purified HCoV-NL63 and  
521 incubated at 32°C for 1 h. Subsequently, cells were fixed and immunostained for HCoV-  
522 NL63 particles (green) and actin (red). Mock-infected cells were used as control (D). Scale  
523 bar = 10 µm.

524

525 **Fig. 5. Cytotoxicity of Pitstop 2 and MitMAB on LLC-MK2 cells.**

526 Cytotoxicity of the tested endocytosis inhibitors was tested with an XTT assay. Cells were  
527 incubated with control DMSO, 10 µM Pitstop 2, or 10 µM MitMAB for 2 h at 37°C Data on  
528 the y-axis represent viability of the treated cells compared to the untreated reference samples.  
529 The assay was performed in triplicate and average values with standard errors are presented.

530

531 **Fig 6. Numerical image analysis: clathrin and dynamin inhibitors block HCoV-NL63**

532 **entry.**

533 LLC-Mk2 cells were incubated with DMSO (**B**), 10  $\mu$ M MitMAB (**C**), or 10  $\mu$ M Pitstop 2  
534 (**D**) for 30 min at 37°C, and subsequently inoculated with purified HCoV-NL63 and incubated  
535 for 45 min at 32°C. Confocal images were digitalized, and localization of each virus particle  
536 relative to the cellular membrane was assessed. In panel (**A**) a graph presenting the number of  
537 internalized virus particles relative to number of virions on the cell surface (y axis) is  
538 presented for cells treated with DMSO (control), Pitstop 2 or MitMAB. In panels (**B**), (**C**),  
539 and (**D**) raw data for cells treated with DMSO, Pitstop 2, or MitMAB, respectively, are  
540 presented. Histograms present an average number of virus particles (y axis) vs the distance  
541 from cell surface (x axis). Values  $< 0$  on the x axis indicate that the virus is inside the cell,  
542 while for extracellular virions x value is  $\geq 0$ .

543

544 **Fig 7. Clathrin and dynamin inhibitors prevent HCoV-NL63 from entering the cell in**  
545 **the HAE model.**

546 HAE were incubated with control DMSO (**A**), 10  $\mu$ M Pitstop 2 (**B**), or 10  $\mu$ M MitMAB (**C**)  
547 for 1 h at 37°C. Further, cells were inoculated with purified HCoV-NL63 and incubated at  
548 32°C for 2 h. Subsequently, cells were fixed and immunostained for HCoV-NL63 particles  
549 (green), actin (red) and nuclei (blue). Scale bar 5  $\mu$ m.

550

551 **Fig. 8. Cytotoxicity of Pitstop 2 and MitMAB on HAE cultures.**

552 Cytotoxicity of the tested endocytosis inhibitors was tested with an XTT assay. Cells were  
553 incubated with control DMSO, 10  $\mu$ M Pitstop 2, or 10  $\mu$ M MitMAB for 2 h at 37°C. Data on  
554 the y-axis represent viability of the treated cells compared to the untreated reference samples.  
555 The assay was performed in triplicate and average values with standard errors are presented.

556

557 **Fig 9. Clathrin and dynamin inhibitors limit the number of LLC-MK2 infected cells.**

558 LLC-Mk2 cells were incubated with control DMSO (A), 5 ug/ml nystatin (B), 10  $\mu$ M  
559 MitMAB (C), 10  $\mu$ M Pitstop 2 (D) for 1 h at 37°C and inoculated with HCoV-NL63  
560 (TCID<sub>50</sub> = 100/ml). After 2 h incubation at 32°C, virions that were not internalized were  
561 inactivated with acidic buffer (pH = 3) and cells were incubated for 4 days at 32°C in the  
562 presence of tested inhibitors or control DMSO. Identical procedure was applied to cells  
563 presented in panels E and F, yet in these MitMAB and Pitstop 2 were applied, respectively,  
564 after the acid wash. Fixed cells were immunostained with anti-NL63 nucleocapsid protein  
565 (green) and nuclei (blue) and confocal images were collected. Scale bar: 200  $\mu$ m.

566

567 **Fig. 10. Clathrin and dynamin inhibitors hamper replication of HCoV-NL63 in LLC-**  
568 **MK2 cells.**

569 (A) HCoV-NL63 replication in LLC-Mk2 cells and HAE cultures in the presence of entry  
570 inhibitors or control DMSO was analyzed using RT-qPCR. Cultures were incubated with  
571 10  $\mu$ M Pitstop 2, 10  $\mu$ M MitMAB, 5 ug/ml nystatin or DMSO for 1 h at 37°C and inoculated  
572 with HCoV-NL63 (TCID<sub>50</sub> = 400/ml). After 2 h incubation at 32°C, virions that were not  
573 internalized were inactivated with acidic buffer (pH = 3) and cells were incubated for 5 days  
574 at 32°C. The data are presented as Log Reduction Value (LRV), compared to the control  
575 sample. The assay was performed in triplicate, and average values with standard errors are  
576 presented. *P* values < 0.05 were considered significant and are denoted with an asterisk (\*).  
577 (B) Cytotoxicity of the tested inhibitors was tested with an XTT assay. Cells were incubated  
578 with 10  $\mu$ M Pitstop 2, 10  $\mu$ M MitMAB, 5 ug/ml nystatin or DMSO for 5 days at 32°C. Data  
579 on the y-axis represent viability of the treated cells compared to the untreated reference

580 samples. The assay was performed in triplicate and average values with standard errors are  
581 presented.

582

583 **Fig 11. Tmprss2 is required for entry to HAE cells, but not enables virus – cell fusion**  
584 **on the cell surface.**

585 (A) HCoV-NL63 replication in LLC-Mk2 cells and HAE cultures in the presence of camostat  
586 or control DMSO was analyzed using RT-qPCR. Cultures were incubated with 100  $\mu$ M  
587 camostat or DMSO for 1 h at 37°C and inoculated with HCoV-NL63 (TCID<sub>50</sub> = 400/ml).  
588 After 2 h incubation at 32°C, virions that were not internalized were inactivated with acidic  
589 buffer (pH = 3) and cells were incubated for 5 days at 32°C. The data are presented as Log  
590 Reduction Value (LRV), compared to the control sample. The assay was performed in  
591 triplicate, and average values with standard errors are presented. *P* values < 0.05 were  
592 considered significant and are denoted with an asterisk (\*). (B) HAE were incubated with  
593 control DMSO or 100  $\mu$ M camostat for 1 h at 37°C. Further, cells were inoculated with  
594 purified HCoV-NL63 and incubated at 32°C for 2 h. Subsequently, cells were fixed and  
595 immunostained for HCoV-NL63 particles (green), actin (red) and nuclei (blue). Scale bar =  
596 5  $\mu$ m.

597

598 **Fig 12. Actin is important for HCoV-NL63 entry.**

599 LLC-MK2 cells were incubated with DMSO (A), 10  $\mu$ M cytochalasin D (B and E), 1.5  $\mu$ M  
600 jasplakinolide (C and F), or 400 nM nocodazole (D and G) for 1 hour at 37°C and inoculated  
601 with purified HCoV-NL63 and incubated at 32°C for 1 h. Actin and virus localization was  
602 verified with confocal microscopy; fixed cells were immunostained for HCoV-NL63 particles  
603 (green), actin (red) and nuclei (blue). Scale bar = 10  $\mu$ m.

604

605 **Fig. 13. Cytotoxicity of the cytoskeleton modifying compounds.**

606 Cytotoxicity of the tested endocytosis inhibitors was tested with an XTT assay. Cells were  
607 incubated with DMSO, 10  $\mu$ M cytochalasin D, 1.5  $\mu$ M jasplakinolide, or 400 nM nocodazole  
608 for 2 h at 37°C. Data on the y-axis represent viability of the treated cells compared to the  
609 untreated reference samples. The assay was performed in triplicate and average values with  
610 standard errors are presented.

611

612 **Fig 14. Early events during HCoV-NL63 infection.**

613

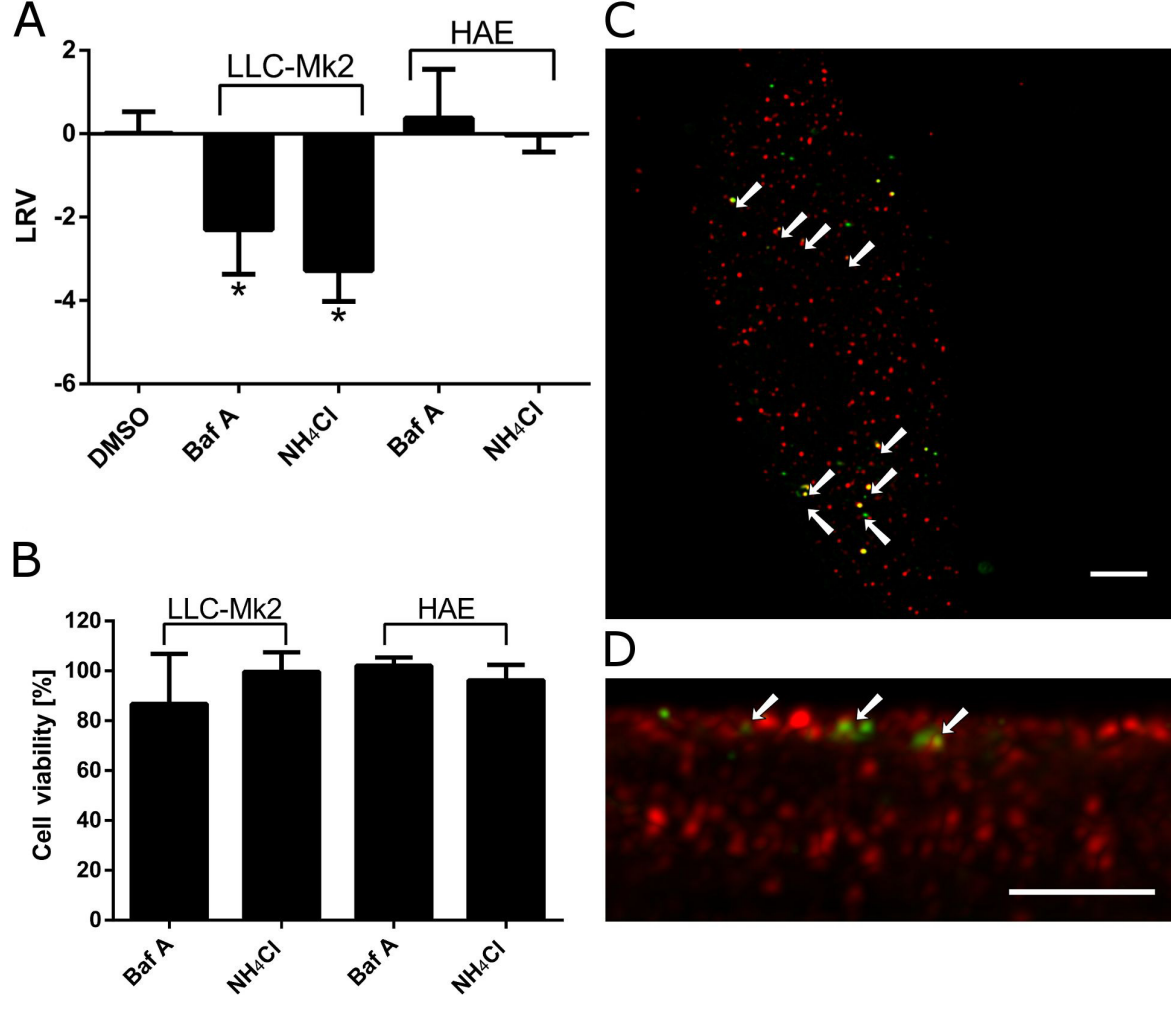
614 **Reference list**

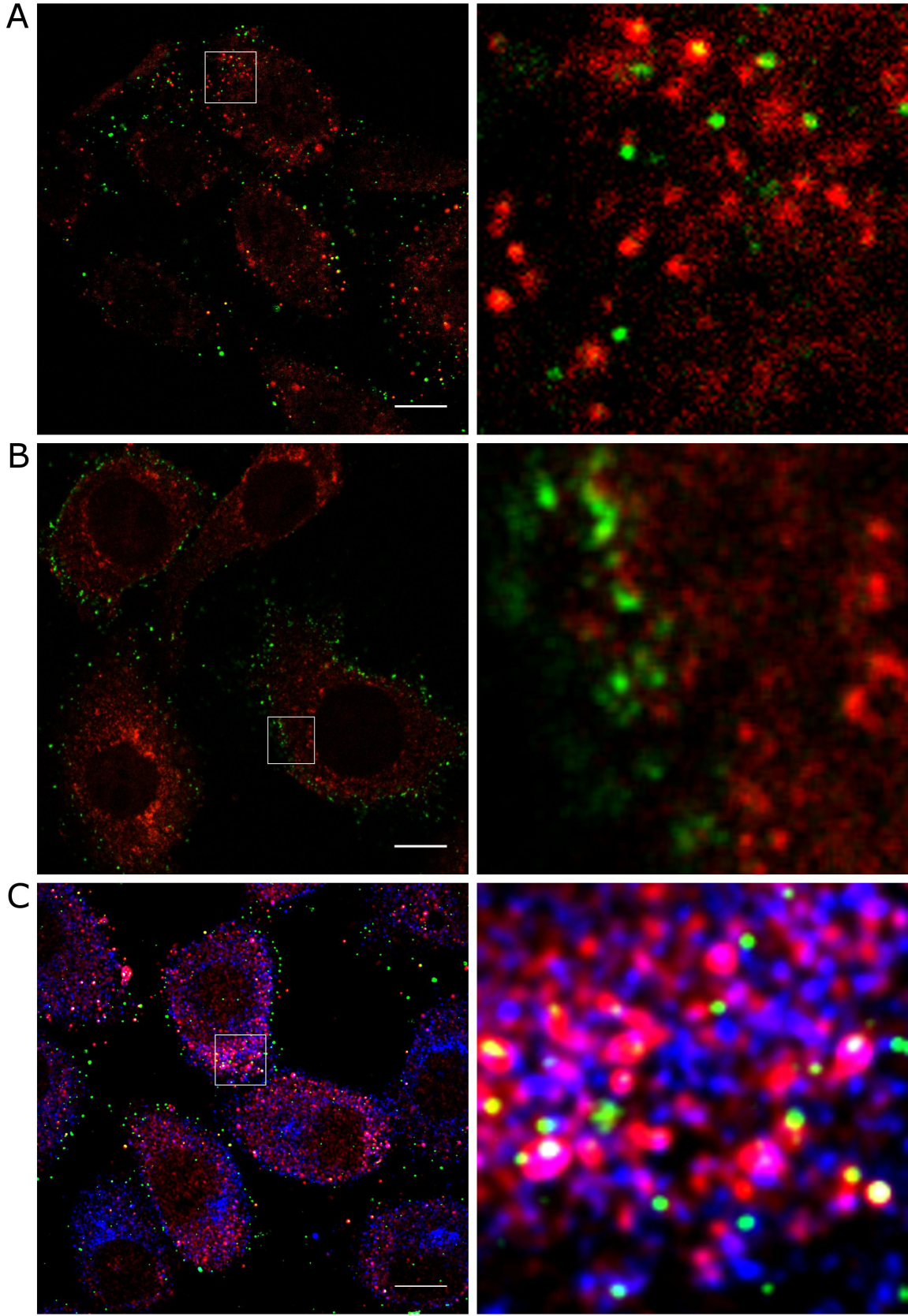
615

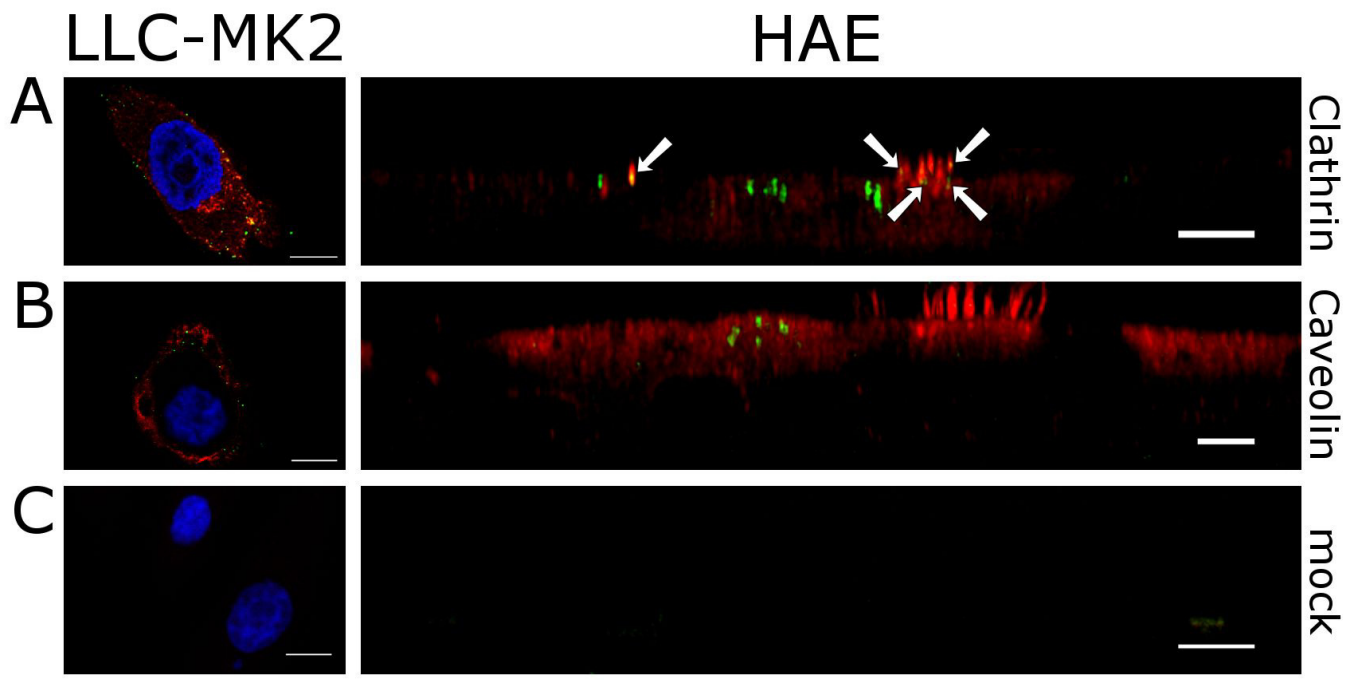
- 616 1. van der Hoek L, Pyrc K, Jebbink MF, Vermeulen-Oost W, Berkhout RJ, Wolthers KC,  
617 Wertheim-van Dillen PM, Kaandorp J, Spaargaren J, Berkhout B. 2004. Identification of a new  
618 human coronavirus. *Nat Med* 10:368-73.
- 619 2. Konca C, Korukluoglu G, Tekin M, Almis H, Bucak İ, Uygun H, Altas AB, Bayrakdar F. 2017. The  
620 First Infant Death Associated With Human Coronavirus NL63 Infection. *Pediatr Infect Dis J*  
621 36:231-233.
- 622 3. Mayer K, Nellessen C, Hahn-Ast C, Schumacher M, Pietzonka S, Eis-Hübinger AM, Drosten C,  
623 Brossart P, Wolf D. 2016. Fatal outcome of human coronavirus NL63 infection despite  
624 successful viral elimination by IFN-alpha in a patient with newly diagnosed ALL. *Eur J*  
625 *Haematol* 97:208-210.
- 626 4. Cabeça TK, Bellei N. 2012. Human coronavirus NL-63 infection in a Brazilian patient  
627 suspected of H1N1 2009 influenza infection: description of a fatal case. *J Clin Virol* 53:82-4.
- 628 5. Oosterhof L, Christensen CB, Sengeløv H. 2010. Fatal lower respiratory tract disease with  
629 human corona virus NL63 in an adult haematopoietic cell transplant recipient. *Bone Marrow*  
630 *Transplant* 45:1115-6.
- 631 6. Fouchier RA, Hartwig NG, Bestebroer TM, Niemeyer B, de Jong JC, Simon JH, Osterhaus AD.  
632 2004. A previously undescribed coronavirus associated with respiratory disease in humans.  
633 *Proc Natl Acad Sci U S A* 101:6212-6.
- 634 7. Pyrc K, Berkhout B, van der Hoek L. 2007. The novel human coronaviruses NL63 and HKU1. *J*  
635 *Virol* 81:3051-7.
- 636 8. van der Hoek L, Sure K, Ihorst G, Stang A, Pyrc K, Jebbink MF, Petersen G, Forster J, Berkhout  
637 B, Uberla K. 2005. Croup is associated with the novel coronavirus NL63. *PLoS Med* 2:e240.
- 638 9. van der Hoek L, Pyrc K, Berkhout B. 2006. Human coronavirus NL63, a new respiratory virus.  
639 *FEMS Microbiol Rev* 30:760-73.
- 640 10. Pyrc K, Dijkman R, Deng L, Jebbink MF, Ross HA, Berkhout B, van der Hoek L. 2006. Mosaic  
641 structure of human coronavirus NL63, one thousand years of evolution. *J Mol Biol* 364:964-  
642 73.

- 643 11. Huynh J, Li S, Yount B, Smith A, Sturges L, Olsen JC, Nagel J, Johnson JB, Agnihothram S, Gates  
644 JE, Frieman MB, Baric RS, Donaldson EF. 2012. Evidence supporting a zoonotic origin of  
645 human coronavirus strain NL63. *J Virol* 86:12816-25.
- 646 12. Tao Y, Shi M, Chommanard C, Queen K, Zhang J, Markotter W, Kuzmin IV, Holmes EC, Tong S.  
647 2017. Surveillance of Bat Coronaviruses in Kenya Identifies Relatives of Human Coronaviruses  
648 NL63 and 229E and Their Recombination History. *J Virol* 91.
- 649 13. Fields BN, Knipe DM, Howley PM. 2013. *Fields virology*, 6th ed. Wolters Kluwer  
650 Health/Lippincott Williams & Wilkins, Philadelphia.
- 651 14. Hofmann H, Pyrc K, van der Hoek L, Geier M, Berkhout B, Pöhlmann S. 2005. Human  
652 coronavirus NL63 employs the severe acute respiratory syndrome coronavirus receptor for  
653 cellular entry. *Proc Natl Acad Sci U S A* 102:7988-93.
- 654 15. Li W, Moore MJ, Vasilieva N, Sui J, Wong SK, Berne MA, Somasundaran M, Sullivan JL,  
655 Luzuriaga K, Greenough TC, Choe H, Farzan M. 2003. Angiotensin-converting enzyme 2 is a  
656 functional receptor for the SARS coronavirus. *Nature* 426:450-4.
- 657 16. Wickramasinghe IN, de Vries RP, Gröne A, de Haan CA, Verheije MH. 2011. Binding of avian  
658 coronavirus spike proteins to host factors reflects virus tropism and pathogenicity. *J Virol*  
659 85:8903-12.
- 660 17. Promkuntod N, Wickramasinghe IN, de Vriese G, Gröne A, Verheije MH. 2013. Contributions  
661 of the S2 spike ectodomain to attachment and host range of infectious bronchitis virus. *Virus*  
662 Res 177:127-37.
- 663 18. Pöhlmann S, Gramberg T, Wegele A, Pyrc K, van der Hoek L, Berkhout B, Hofmann H. 2006.  
664 Interaction between the spike protein of human coronavirus NL63 and its cellular receptor  
665 ACE2. *Adv Exp Med Biol* 581:281-4.
- 666 19. Milewska A, Zarebski M, Nowak P, Stozek K, Potempa J, Pyrc K. 2014. Human coronavirus  
667 NL63 utilizes heparan sulfate proteoglycans for attachment to target cells. *J Virol* 88:13221-  
668 30.
- 669 20. Mathewson AC, Bishop A, Yao Y, Kemp F, Ren J, Chen H, Xu X, Berkhout B, van der Hoek L,  
670 Jones IM. 2008. Interaction of severe acute respiratory syndrome-coronavirus and NL63  
671 coronavirus spike proteins with angiotensin converting enzyme-2. *J Gen Virol* 89:2741-5.
- 672 21. Yoshimori T, Yamamoto A, Moriyama Y, Futai M, Tashiro Y. 1991. Bafilomycin A1, a specific  
673 inhibitor of vacuolar-type H(+)-ATPase, inhibits acidification and protein degradation in  
674 lysosomes of cultured cells. *J Biol Chem* 266:17707-12.
- 675 22. Misinzo G, Delputte PL, Nauwynck HJ. 2008. Inhibition of endosome-lysosome system  
676 acidification enhances porcine circovirus 2 infection of porcine epithelial cells. *J Virol*  
677 82:1128-35.
- 678 23. Richards AL, Jackson WT. 2012. Intracellular vesicle acidification promotes maturation of  
679 infectious poliovirus particles. *PLoS Pathog* 8:e1003046.
- 680 24. Milewska A, Ciejka J, Kaminski K, Karewicz A, Bielska D, Zeglen S, Karolak W, Nowakowska M,  
681 Potempa J, Bosch BJ, Pyrc K, Szczubialka K. 2013. Novel polymeric inhibitors of HCoV-NL63.  
682 *Antiviral Res* 97:112-21.
- 683 25. Mu FT, Callaghan JM, Steele-Mortimer O, Stenmark H, Parton RG, Campbell PL, McCluskey J,  
684 Yeo JP, Tock EP, Toh BH. 1995. EEA1, an early endosome-associated protein. EEA1 is a  
685 conserved alpha-helical peripheral membrane protein flanked by cysteine "fingers" and  
686 contains a calmodulin-binding IQ motif. *J Biol Chem* 270:13503-11.
- 687 26. Dutta D, Williamson CD, Cole NB, Donaldson JG. 2012. Pitstop 2 is a potent inhibitor of  
688 clathrin-independent endocytosis. *PLoS One* 7:e45799.
- 689 27. Joshi S, Perera S, Gilbert J, Smith CM, Mariana A, Gordon CP, Sakoff JA, McCluskey A,  
690 Robinson PJ, Braithwaite AW, Chircop M. 2010. The dynamin inhibitors MiTMAB and  
691 OcTMAB induce cytokinesis failure and inhibit cell proliferation in human cancer cells. *Mol*  
692 *Cancer Ther* 9:1995-2006.
- 693 28. Schnell JR, Chou JJ. 2008. Structure and mechanism of the M2 proton channel of influenza A  
694 virus. *Nature* 451:591-5.

- 695 29. Eckels PC, Banerjee A, Moore EE, McLaughlin NJ, Gries LM, Kelher MR, England KM,  
696 Gamboni-Robertson F, Khan SY, Silliman CC. 2009. Amantadine inhibits platelet-activating  
697 factor induced clathrin-mediated endocytosis in human neutrophils. *Am J Physiol Cell Physiol*  
698 297:C886-97.
- 699 30. Chen Y, Wang S, Lu X, Zhang H, Fu Y, Luo Y. 2011. Cholesterol sequestration by nystatin  
700 enhances the uptake and activity of endostatin in endothelium via regulating distinct  
701 endocytic pathways. *Blood* 117:6392-403.
- 702 31. Shirato K, Kanou K, Kawase M, Matsuyama S. 2017. Clinical Isolates of Human Coronavirus  
703 229E Bypass the Endosome for Cell Entry. *J Virol* 91.
- 704 32. Reinke LM, Spiegel M, Plegge T, Hartleib A, Nehlmeier I, Gierer S, Hoffmann M, Hofmann-  
705 Winkler H, Winkler M, Pöhlmann S. 2017. Different residues in the SARS-CoV spike protein  
706 determine cleavage and activation by the host cell protease TMPRSS2. *PLoS One*  
707 12:e0179177.
- 708 33. Casella JF, Flanagan MD, Lin S. 1981. Cytochalasin D inhibits actin polymerization and induces  
709 depolymerization of actin filaments formed during platelet shape change. *Nature* 293:302-5.
- 710 34. Holzinger A. 2009. Jasplakinolide: an actin-specific reagent that promotes actin  
711 polymerization. *Methods Mol Biol* 586:71-87.
- 712 35. Hopkins CR, Miller K, Beardmore JM. 1985. Receptor-mediated endocytosis of transferrin and  
713 epidermal growth factor receptors: a comparison of constitutive and ligand-induced uptake. *J*  
714 *Cell Sci Suppl* 3:173-86.
- 715 36. Warren RA, Green FA, Enns CA. 1997. Saturation of the endocytic pathway for the transferrin  
716 receptor does not affect the endocytosis of the epidermal growth factor receptor. *J Biol*  
717 *Chem* 272:2116-21.
- 718 37. Ferguson SM, De Camilli P. 2012. Dynamin, a membrane-remodelling GTPase. *Nat Rev Mol*  
719 *Cell Biol* 13:75-88.
- 720 38. Park JE, Li K, Barlan A, Fehr AR, Perlman S, McCray PB, Gallagher T. 2016. Proteolytic  
721 processing of Middle East respiratory syndrome coronavirus spikes expands virus tropism.  
722 *Proc Natl Acad Sci U S A* 113:12262-12267.
- 723 39. MacLean-Fletcher S, Pollard TD. 1980. Mechanism of action of cytochalasin B on actin. *Cell*  
724 20:329-41.
- 725 40. Reed L, Muench H. 1938. A simple method of estimating fifty per cent endpoints., p 493-497.  
726 *Am. J. Epidemiol.*
- 727 41. Harding C, Heuser J, Stahl P. 1983. Receptor-mediated endocytosis of transferrin and  
728 recycling of the transferrin receptor in rat reticulocytes. *J Cell Biol* 97:329-39.
- 729 42. Schubert W, Frank PG, Razani B, Park DS, Chow CW, Lisanti MP. 2001. Caveolae-deficient  
730 endothelial cells show defects in the uptake and transport of albumin in vivo. *J Biol Chem*  
731 276:48619-22.
- 732 43. Berniak K, Rybak P, Bernas T, Zarębski M, Biela E, Zhao H, Darzynkiewicz Z, Dobrucki JW.  
733 2013. Relationship between DNA damage response, initiated by camptothecin or oxidative  
734 stress, and DNA replication, analyzed by quantitative 3D image analysis. *Cytometry A* 83:913-  
735 24.
- 736







# Transferrin

DMSO

Pitstop

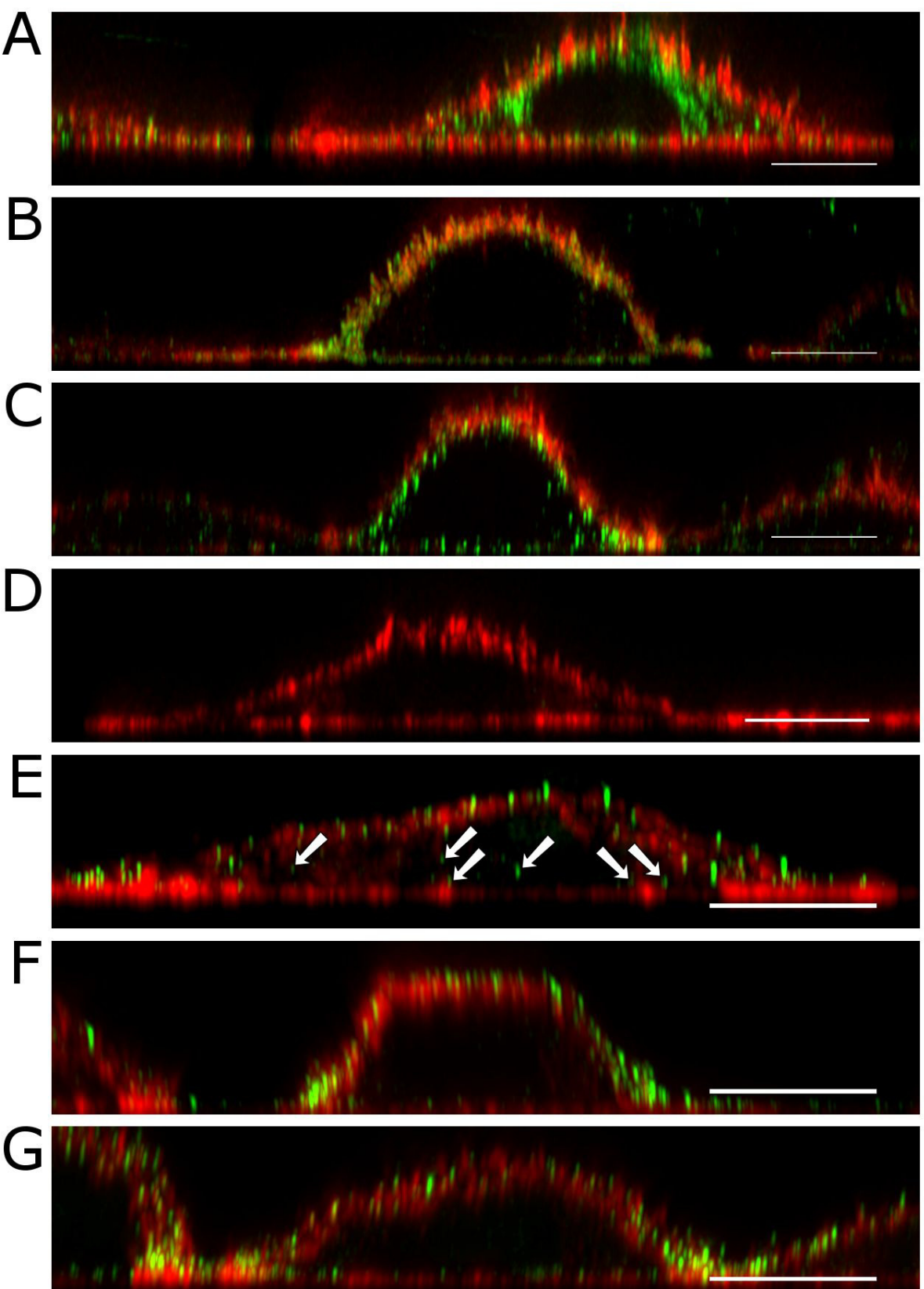
MITTMAB

Control

DMSO

Pitstop

MITTMAB



# HCoV-NL63

